# The role of composition in the combustion of n-heptane/iso-butanol mixtures: experiments and detailed modelling

Alireza Dalili , Jordan D. Brunson , Songtao Guo , Massimiliano Turello , Fabio Pizzetti , Lucia Badiali , Charles T. Avedisian , Kalyanasundaram Seshadri , Alberto Cuoci , Forman A. Williams , Alessio Frassoldati & Michael C. Hicks

Taylor & Francis
Taylor & Francis Group

Check for updates

# The role of composition in the combustion of n-heptane/iso-butanol mixtures: experiments and detailed modelling

Alireza Dalili[a], Jordan D. Brunson[a], Songtao Guo[a], Massimiliano Turello[b],
Fabio Pizzetti[b], Lucia Badiali[b], Charles T. Avedisian[a*], Kalyanasundaram Seshadri[b],
Alberto Cuoci[c], Forman A. Williams[b], Alessio Frassoldati[c] and Michael C. Hicks[d]

[a]*Sibley School of Mechanical and Aerospace Engineering, Cornell University, Ithaca, NY, USA;*
[b]*Department of Mechanical and Aerospace Engineering, University of California, San Diego, CA,
USA;* [c]*Dipartimento di Chimica, Materiali e Ingegneria Chimica, Politecnico di Milano, Milano,
Italy;* [d]*National Aeronautics and Space Administration, Glenn Research Center, Cleveland, OH,
USA*

Experimental data and detailed numerical modelling are presented on the burning characteristics of a model gasoline/biofuel mixture consisting of n-heptane and iso-butanol. A droplet burning in an environment that minimises the influence of buoyant and forced convective flows in the standard atmosphere is used to promote one-dimensional gas transport to facilitate numerical modelling of the droplet burning process. The numerical model includes a detailed combustion kinetic mechanism, unsteady gas and liquid transport, multicomponent diffusion inside the droplet, variable properties, and non-luminous radiative heat transfer from the flame. The numerical simulation was validated by experimental measurements in the standard atmosphere which showed good agreement with the evolutions of droplet and flame diameters. The iso-butanol concentration had a strong effect on formation of particulates. Above 20% (volume) iso-butanol, flame luminosity was significantly diminished and decreased with increasing iso-butanol concentration, while $CO_2$ emissions as a representative greenhouse gas were not strongly influenced by the iso-butanol loading. The soot shell was located near a 1350 K isotherm for concentrations up to 20% (volume) iso-butanol, suggesting this value as a possible soot inception temperature for the mixture droplet. The combustion rate decreased with increasing iso-butanol concentration which was attributed to iso-butanol's higher liquid density. No evidence of a low temperature burning regime, or of extinction, was found (in experiments and simulations) for the small droplet sizes investigated.

**Keywords:** droplet combustion; biofuel; droplet; combustion; surrogate; n-heptane; iso-butanol

## 1. Introduction

Gasoline and diesel fuel have powered combustion engines for over a century and they will continue to be the dominant fuel for the ground transportation fleet for the foreseeable future [1,2]. Crude oil supplies are not unlimited, however. When they are sufficiently depleted oxygenated biofuels mixed with gasoline or diesel are a viable alternative to

---

Table 1.  Selected Properties [22].

| Property | n-Heptane | Iso-butanol |
|---|---|---|
| Formula | $C_7H_{16}$ | $C_4H_{10}O$ |
| Boiling Point (K) | 372 | 381 |
| Molecular Weight (g/mole) | 100.2 | 74.1 |
| Density (@297.7 K, kg/m$^3$) | 680 | 802 |
| Heat of vaporisation (@$T_b$, J/kg) | $31.7 \times 10^4$ | $56.6 \times 10^4$ |

mitigate the depletion of petroleum reserves while also reducing particulate formation and effects on global warming.

Ethanol is the most common and familiar biofuel additive to gasoline. The deleterious environmental impacts of ethanol production [3] have motivated the search for alternatives. A so-called 'merit function' was recently developed to assist the process of finding alternative additives to gasoline [4]. Iso-butanol ($C_4H_{10}O$, boiling point of 381 K) in particular has been shown to be a promising alternative for this purpose [5] because it has a higher energy density and lower hygroscopicity than ethanol [6]. However, little is known about the combustion of gasoline and iso-butanol mixtures.

The present study considers the combustion of a model petroleum fuel/biofuel mixture consisting of iso-butanol mixed with n-heptane. N-heptane is relevant to both gasoline and diesel because it is a primary-reference-fuel component for gasoline and it has also been used to represent the kinetic mechanism of diesel fuel [7–9]. Table 1 shows selected properties.

The configuration of an isolated droplet burning with spherical symmetry is used in the present study to access the thermochemical processes of liquid fuel burning. A burning droplet incorporates multiphase effects and liquid evaporation, and the spherically symmetric configuration is amenable to detailed numerical modelling. The 1-D droplet burning configuration in particular has been shown to be valuable for understanding salient features of the fuel burning process and for assisting with modelling distillation curves for developing surrogates for complex miscible mixtures such as fuels for advanced combustion engines [8].

No prior work is known to have been reported on the droplet burning characteristics of *n*-heptane/iso-butanol mixtures. Experimental data and detailed numerical modelling are reported in this paper which fill this gap. New data and analysis are reported on the role of iso-butanol mixture fraction on the physicochemical aspects of droplet burning including gaseous emissions and fuel burn rates. Detailed modelling provides the ability to validate kinetic mechanisms and property inputs to the simulation for a multiphase configuration not normally considered in such validation efforts.

Because iso-butanol is an oxygenated fuel, it is expected to influence sooting propensity. A mechanism has been offered for oxygenated molecules that involves carbon atoms remaining bonded to oxygen atoms when the oxygenate is mixed with the fuel [11]. The sooting propensity of the blend is reduced because the carbon atoms are not then available to be transformed into soot. The effect of iso-butanol mixture fraction on sooting propensity is addressed here through predictions of a soot precursor species (acetylene) as well as through more qualitative experimental measures associated with incandescence from soot particles in the droplet flames.

The spherically symmetric droplet burning configuration that promotes a one-dimensional transport configuration is amenable to detailed numerical modelling. No other

liquid fuel combustion configuration with as close a connection to a spray flame (which sets initial conditions for combustion in engines [1]) has this modelling potential. For the 1-D droplet flame, the gas flow is entirely the result of fuel evaporation and the flame is spherical and symmetrically positioned around the droplet. Any soot that forms collects in a shell-like structure on the fuel-rich side of the flame by the forces (thermophoresis and Stefan drag) acting on the soot aggregates.

Detailed numerical modelling of 1-D droplet flames has provided insights into several features of burning of liquid fuels, including cool-flame behaviour, soot formation, and preferential vaporisation effects [12–16]. The 1-D droplet flame has the potential to provide benchmark data for validating chemical-kinetic inputs and property databases to detailed numerical solvers. Such data are provided here for the heptane/iso-butanol system. The next sections describe the experimental methodology, followed by a presentation of the numerical model and a discussion of the experimental and numerical results.

## 2.   Experimental methodology and diagnostics

Spherical symmetry in the burning process is promoted by burning droplets in a stationary atmosphere, anchoring the droplets so that they do not move, and having the burning process take place in an environment of low gravity to minimise buoyancy during the experiments. Details of how this environment is created are discussed in [10,17] and briefly outlined here.

Test droplets were deployed within a sealed chamber in the standard atmosphere and then placed in free-fall before being ignited to minimise buoyant effects. The free-fall distance was 7.6 m which provided approximately 1.2 s of experimental test time. This time was sufficient to observe the complete burning history for droplets with initial diameters in the range of 0.5 to 0.6 mm. The instrumentation package impacted a 1.8 m diameter by 1.8 m tall cylindrical tank partially filled with foam.

The droplets were anchored to two 14 $\mu$m SiC fibres to prevent the droplets from moving. The fibers did not influence the burning process [18]. Ignition was by two sparks positioned on opposite sides of the droplet. The spark discharges were created by electronic circuitry that controlled the energy imparted to the sparks and allowed for measuring the spark durations.

The experimental diagnostic of the experiments was digital video imaging. Other options such as laser-based instrumentation were not employed because of the challenge of maintaining optical alignment upon impact in the deceleration tank at the conclusion of the experiment. Two video cameras were employed: a black-and-white (BW) camera for recording the droplet and soot morphology and a colour camera for recording the flame. Backlighting was provided for the BW camera using a single wavelength LED (Prismatix Mic-LED with BLCC-04; 637 nm). With video imaging being the main diagnostic, image analysis tools had to be used to extract quantitative data from the video images.

Video images were processed with computer software to extract quantitative measurements of the droplet and flame diameters. Black-and-white images were analysed by a previously developed MATLAB-based algorithm [19], which iteratively converges on a measurement of the droplet's diameter through edge-detection methods. The sooting propensities of the mixtures were found to be minimal for the n-heptane/iso-butanol system under the present experimental conditions, and soot is not included in the simulation.

Flame and soot shell diameters were more challenging to measure because of their comparatively less well defined boundary and image contrast with the surrounding. In fact, no

soot shell diameter measurements could be obtained at all owing to the faintly defined shell structure above about 10% iso-butanol concentration. As a result, and unlike the droplet images themselves, flame diameter measurements had to be made by a manual method. A commercial software analysis tool was used for this purpose (ImagePro Plus, Rockville, MD).

Flame diameters were measured from colour images with the aid of the ImagePro Plus software package. Because the flame boundary was not sharp enough as shown in Figure 4(b) for automated processing algorithms to be used, flame diameter measurements were made using a manual process. The method consisted of manually placing a virtual ellipse around the outer blue-hued luminous boundary of unprocessed video images and measuring the major (a) and minor (b) axes to obtain an equivalent flame diameter as $D_f = (a \times b)^{1/2}$. The outer edge of the blue zone is the important boundary to consider in placement of the virtual ellipse. Several approaches were investigated for improving measurements, including using image enhancement and intensity profile tools of the image analysis software. Diameters obtained using these alternatives to working with unprocessed heptane/iso-butanol flame images did not provide added benefit. Furthermore, measurements were routinely checked between different individuals for consistency.

The fuel droplets featured in this study were ignited with a minimal amount of energy. The minimum energy level was first determined through successive tests in the laboratory framework to find the lowest spark settings at which droplets would ignite. Using the measured spark currents and voltages, the minimum energy was defined by the following formulation for a two-spark configuration:

$$E_{\min} = \int_0^\tau (V_1(t)I_1(t) + V_2(t)I_2(t)) \, \mathrm{d}t \qquad (1)$$

where the product of the voltages ($V_1$ and $V_2$) and currents ($I_1$ and $I_2$) were integrated over the duration of the sparks $\tau$. Spark voltages and currents were measured by an oscilloscope (Lecroy waveRunner 6050A) at a sampling rate of 25 MS/s. Since the data gathered are discrete, Equation (1) was evaluated in the form

$$E_{\min} \approx \sum_{n=1}^{n_{samples}} (V_{1,n}I_{1,n} + V_{2,n}I_{2,n}) \, \Delta t \qquad (2)$$

where $\Delta t$ is the time interval per sample. Figures 1 and 2 show the measurements. The spark energy depends on both the geometrical placement of the droplet relative to the spark kernel and the spark duration. The data in Figures 1 and 2 are specific to the geometry shown in the inset to Figure 1.

The trends show that more energy and longer spark durations were required to ignite iso-butanol droplets. In a sense, iso-butanol was more difficult to ignite than heptane. Considering the properties in Table 1, this trend can be a reflection of differences in the heats of vaporisation of heptane and iso-butanol, with iso-butanol having an over 25% higher value than heptane.

It was previously noted that exposure of mixture droplets to the ambient atmosphere prior to ignition could lead to a compositional change of a droplet through preferential vaporisation [10]. Appendix A discusses the methodology for assessing this potential problem for the n-heptane/iso-butanol mixture. For the experiments outlined in this paper, the exposure time of the droplets to air prior to ignition was limited to approximately 2 s which is short enough that this is not a consideration.
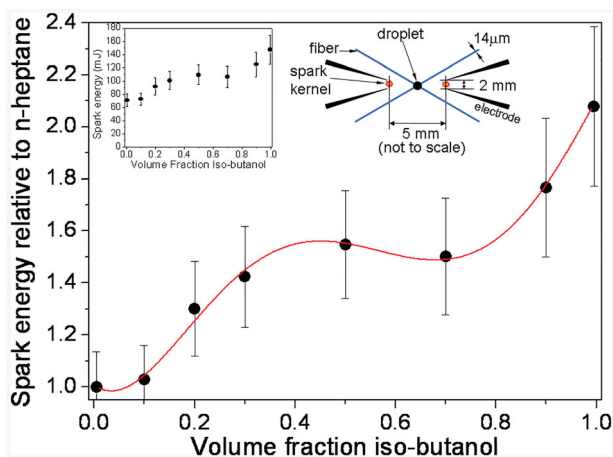
Figure 1. The minimum ignition energy as a function of the iso-butanol volume fraction for the configuration in the inset. Ignition energies are dependent on proximity of the droplet to the spark kernel. The data are given in the Supplementary Material section.
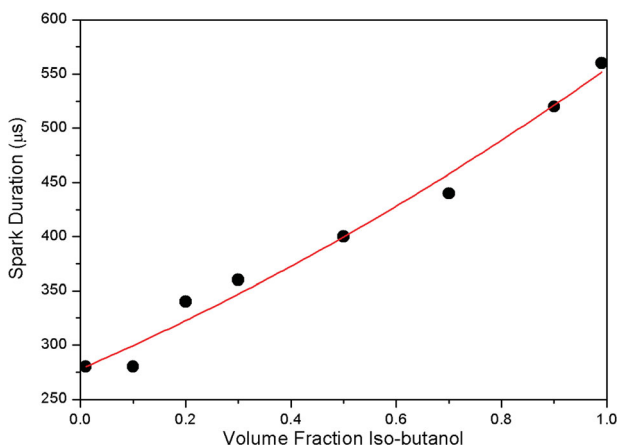


Figure 2. The spark duration as a function of the iso-butanol volume fraction. A trend line is shown.

Experiments were carried out for the following mixture volume fractions: (n-heptane/iso-butanol): 10/90, 30/70, 50/50, 70/30, 80/20, and 90/10. In practice, the iso-butanol mixture fraction in gasoline may be restricted. For example, the iso-butanol loading in gasoline has been recommended to be about 16% volume fraction [5] based on iso-butanol at this concentration providing the same oxygen content as ethanol in commercial E10 (i.e. 10% ethanol mixed with 90% gasoline). Nonetheless, varying the composition over the entire range of mixture fractions provides a more complete understanding of iso-butanol's influence on combustion.

## 3. Detailed numerical modeling

The conservation equations of mass and energy were solved numerically in the spherical coordinate system to simulate the droplet burning process. The model included variable gas

and liquid thermal and transport properties that depended on composition and temperature, and detailed combustion chemistry with soot precursors among the species. A model for soot formation was not included because of an expected lack of a strong sooting propensity for the mixture and the computational cost involved. Previous detailed modelling of small n-heptane droplet burning at atmospheric pressure showed good agreement with experiments when a soot model was not included in the analysis [20]. For burning at elevated pressures a soot model would likely be needed in anticipation of the increased sooting propensity. Energy loss by non-luminous, optically thin and transparent-gases (primarily from $CO_2$ and $H_2O$ bands) was included in the simulation.

The transport equations solved were as follows. For the liquid phase ($0 < r < R_d$) radial convection, species diffusion and heat conduction were included. The mass, energy and species conservation equations are

$$\frac{\partial \rho_L}{\partial t} + \frac{1}{r^2}\frac{\partial}{\partial r}(r^2 \rho_L v_L) = 0 \tag{3}$$

$$\rho_L c_{p,L}\left(\frac{\partial T_L}{\partial t} + v_L \frac{\partial T_L}{\partial r}\right) = \frac{1}{r^2}\frac{\partial}{\partial r}\left(r^2 k_L \frac{\partial T_L}{\partial r}\right) \tag{4}$$

and

$$\rho_L\left(\frac{\partial Y_{L,i}}{\partial t} + v_L \frac{\partial Y_{L,i}}{\partial r}\right) = -\frac{1}{r^2}\frac{\partial}{\partial r}(r^2 \rho_L Y_{L,i} V_{L,i}) \tag{5}$$

where the subscript 'i' denotes the species in the liquid ($i = 1,2$), and $\rho_L$ is the mixture liquid density which is dependent on composition and temperature. For the gas surrounding the droplet ($r > R_d$), the one-dimensional form of the mass, energy and species conservation equations are

$$\frac{\partial \rho_g}{\partial t} + \frac{1}{r^2}\frac{\partial}{\partial r}(r^2 \rho_g v_g) = 0 \tag{6}$$

$$\rho_g c_{p,g}\left(\frac{\partial T_g}{\partial t} + v_g \frac{\partial T_g}{\partial r}\right) = \frac{1}{r^2}\frac{\partial}{\partial r}\left(r^2 k_g \frac{\partial T_g}{\partial r}\right) - \rho_g \sum_{i=1}^{N_c}(Y_{g,i} V_{g,i} c_{p,g,i})\frac{\partial T_g}{\partial r}$$

$$- \sum_{i=1}^{N_c}(\omega_{g,i} H_{g,i}) - \frac{1}{r^2}\frac{\partial}{\partial r}\left(r^2 q_R\right) \tag{7}$$

$$\rho_g\left(\frac{\partial Y_{g,i}}{\partial t} + v_g \frac{\partial Y_{g,i}}{\partial r}\right) = -\frac{1}{r^2}\frac{\partial}{\partial r}(r^2 \rho_g Y_{g,i} V_{g,i}) + \omega_{g,i} \tag{8}$$

where the summation is over all chemical species present (the total number being $N_c$) from the reaction at the flame. The term $q_R$ in Equation (7) is non-luminous radiative heat flux. The radiation model described in [21] was used. $V_{L,i}$ and $V_{g,i}$ represent the diffusion velocity of species 'i' in the liquid ('L') or gas ('g'), respectively, incorporating contributions from Fick's law and thermal diffusion (the Soret effect) in a mixture-average description. Details are provided in [23].

The boundary conditions at the droplet centre ($r = 0$), droplet surface ($r = R_d$) and the far field (numerically represented by a radial distance $r = R_\infty$) are

$$\left.\frac{\partial T_L}{\partial r}\right|_{r=0} = 0 \tag{9}$$

$$\left.\frac{\partial Y_{L,i}}{\partial r}\right|_{r=0} = 0 \tag{10}$$

$$k_L \left.\frac{\partial T_L}{\partial r}\right|_{r=R_d^-} + \sum_{i=1}^{N_c} (W_{tot} Y_{g,i} + \rho_g Y_{g,i} V_{g,i}) h_{fg,i} = k_g \left.\frac{\partial T_g}{\partial r}\right|_{r=R_d^+} + q_R \tag{11}$$

$$T_L|_{R_d^-} = T_g|_{R_d^+} \tag{12}$$

$$f_{L,i} = f_{g,i} \tag{13}$$

$$W_{tot} Y_{L,i} - \rho_L \mathfrak{D}_{L,i} \left.\frac{\partial Y_{L,i}}{\partial r}\right|_{r=R_d^-} = W_{tot} Y_{g,i} + \rho_g Y_{g,i} V_{g,i} \tag{14}$$

$$W_{tot} = \rho_g \left( v_g - \frac{dR_d}{dt} \right) \tag{15}$$

where again $i = 1,2$ for a binary liquid ('L') and $i = 1$ to $N_c$ for the gas ('g'), with a surface emissivity of unity. At $r = R_\infty$,

$$T_g = T_g^o \tag{16}$$

$$Y_{g,i} = Y_{g,i}^o \tag{17}$$

Equation (14) expresses the interface species conservation condition associated with the evaporating miscible mixture. Several mixture models were employed for Equation (13), including an ideal liquid mixture with unity activity coefficients (i.e. Raoult's law), and an equation of state (i.e. Peng-Robinson) that involved solving a set of non-linear algebraic equations. Fugacity and activity coefficients (assessed with the UNIFAC method) were close to unity even though the n-heptane/iso-butanol mixture is a non-polar/polar mixture, implying that an ideal mixture model would be adequate for simulating the burning process.

The system of partial differential equations was solved using the method of lines coupled with a spatial discretization via the finite-difference method (based on an adaptive grid fixed on the droplet surface) using the OpenSMOKE++ framework [24,25]. Ignition was modelled by a short period ($\sim 100$ ms) of pure evaporation at ambient temperature, followed by an instantaneous jump to a non-uniform radial temperature profile peaking at $\sim 2200$ K. For the results presented in this study, the burning process did not appear to be strongly influenced by the ignition model.

The kinetic mechanism used here was taken from [26]. This large mechanism was reduced through removal of large molecules, ultimately resulting in a mechanism consisting of 225 species and 7645 reactions. This mechanism does not include low temperature combustion chemistry. Limited simulations were performed with the large detailed
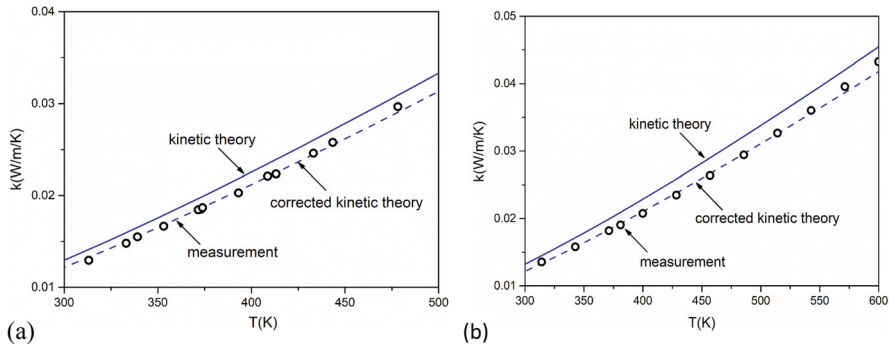
Figure 3. (a) The thermal conductivity of iso-butanol with and without a correction factor, over the temperature range available in [28]. (b) The thermal conductivity of n-heptane with and without a correction factor, over the temperature range available in [29]

mechanism, but no differences were noted. Transport and thermodynamic properties along with mixing rules were taken from the CRECK database [25].

Thermal properties can have a strong influence on simulations as shown in a previous study on burning of butanol isomer droplets [27]. Because of this, the CRECK property database (founded upon the Chapman-Enskog kinetic-theory conductivity prediction, with the Eucken approach to account for rotational and vibrational energies) was tested against measurements available for pure fuel components, with ad-hoc corrections made to improve agreement with the data. Figure 3 shows predicted gas thermal conductivities for iso-butanol and n-heptane. The kinetic-theory predictions were found to be high by 7% to 8%. The predicted conductivities were corrected by this amount to give the dotted lines in Figure 3.

Theoretical predictions were then developed over the complete range of temperatures of interest, with this correction included, and these results were correlated by a polynomial fit to save computational time without sacrificing accuracy.

Because the computational model solves the full set of governing equations, no assumptions are made about the reaction zone and no flame diameter emerges naturally from the simulations. We defined the flame diameter in two ways and report results for both: maximum gas temperature; and maximum OH concentration. Measured flame diameters were generally found to lie between these two definitions as discussed in Section 5. Furthermore, with the assumption of spherical symmetry, the model is not able to consider the possible formation of internal circulation zones.

## 4. Experimental results

Figure 4(a) shows representative backlit BW images, while Figure 4(b) shows colour-camera flame images, mainly soot incandescence, which is a qualitative measure of sooting propensity [30].

It is evident from the flame brightness that adding iso-butanol to n-heptane reduces sooting propensities. Above an iso-butanol concentration of about 20%, the flame incandescence and soot-shell visibility were significantly reduced as seen qualitatively in Figure 4. This trend can be attributed to the oxygenated structure of iso-butanol as discussed further in Section 6.
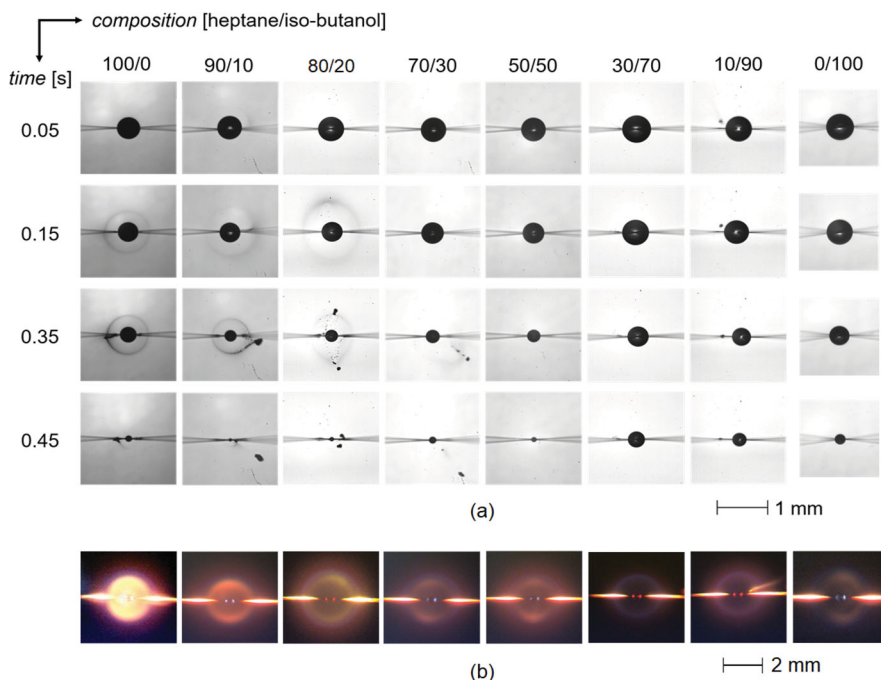
(a)

⊢——————⊣ 1 mm



(b)

⊢——————⊣ 2 mm

Figure 4.　(a) Selected BW image sequences for each composition examined. (b) Selected colour images qualitatively showing the most intense flame emissions for each fuel mixture.

Droplet-burning histories are presented in Figure 5 where the red curves show the droplet diameter in the classical $D^2$-law coordinates [31]. The flame standoff ratio data, FSR $= D_f/D$, are included as black symbols in the figure.

The data in Figure 5 show a very slight time-dependence to the evolution of $D^2$ but a relative position of the flame to the droplet that is strongly time-dependent. These trends are consistent with early theoretical treatments of droplet burning of a single component fuel that considered transient effects and developed solutions to the governing equations in an inner and outer zone [31]. Regarding the flame, the relative positions of the flame to the droplet increase because the droplet regresses faster than the flame because of finite transport effects associated with the flame location readjusting to the changing thermal conditions.

Figure 5 also shows different levels of standard deviations of the flame diameter data for the mixture fractions investigated. There did not appear to be a systematic trend of measurement uncertainty with iso-butanol concentration. The outer luminous boundary was more difficult to discern when the droplets were almost burned out. Moreover, for some of the colour video sequences the outer blue-hued luminous boundary was more visible in the experimental runs than others. Flame image quality and accuracy of measuring the flame diameter was also dependent on flame brightness, quality of the video image and to some extent the filter employed on the colour camera. Reduced visibility of the outer boundary of the flame due to a bright inner core made it more difficult in some cases to discern the flame boundary which decreased the measurement precision and increased the standard deviations in some cases.
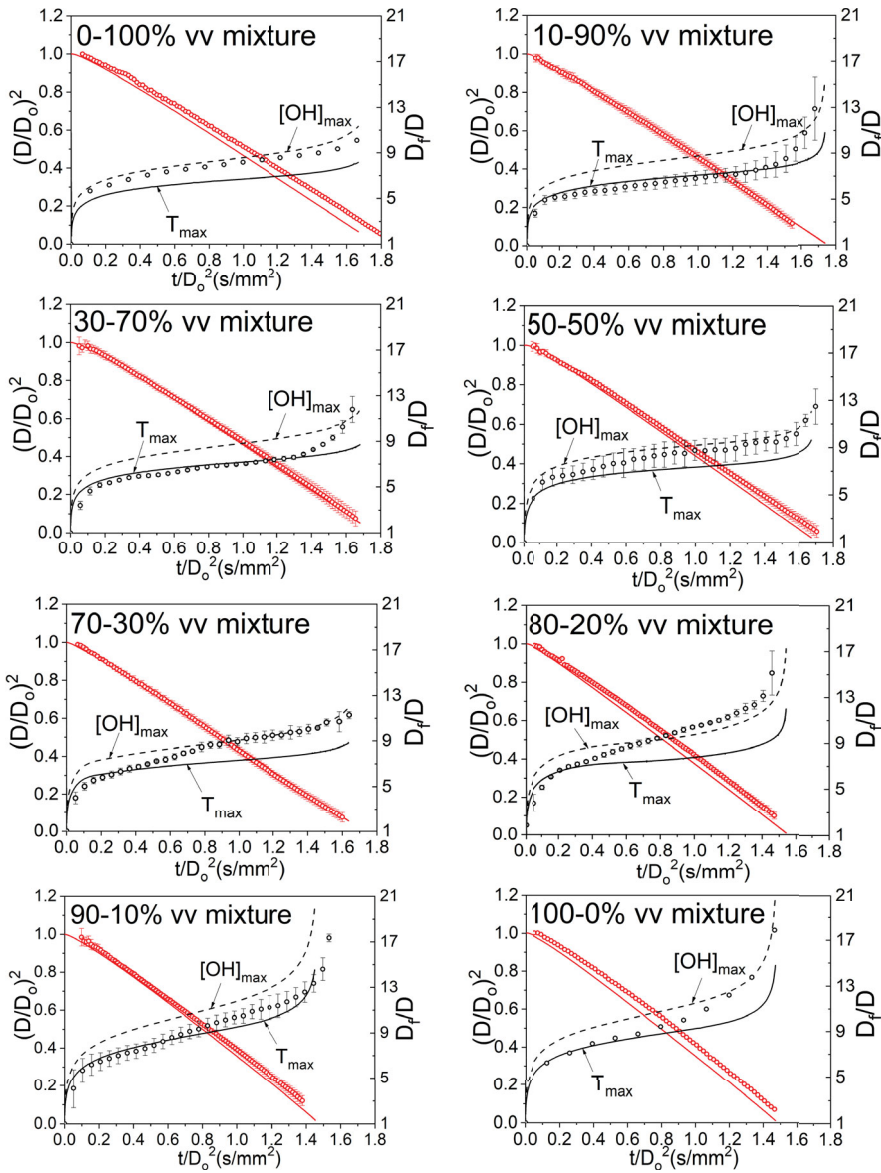
Figure 5. Evolution of droplet and flame diameters for the indicated compositions (volume percent n-heptane/iso-butanol) presented in scaled coordinates. Solid lines are simulations and measurements are symbols. Data are averages of four or five experiments with the standard deviations shown. Flame diameter predictions are based on maximum temperature and OH concentrations. The experimental data are included in the Supplementary Material section.

To illustrate the influence of iso-butanol concentration on mixture burning, a single burning rate was obtained from the data in Figure 5 for each composition. This was done by linearising the data over the most linear portion of the burning histories, $0.4 \, \text{s/mm}^2 < t/D_o^2 < 1.4 \, \text{s/mm}^2$, and cross-plotting the resulting burn rates (defined as $K \equiv$
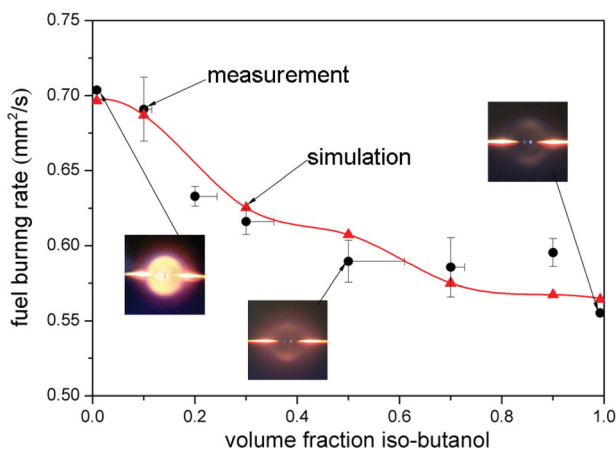
Figure 6. Comparison between measured (circles) and simulated (triangles) burning rates. Representative images of most intense flame emissions are shown for selected compositions. A trend line is shown. The experimental burning rate data are included in the Supplementary Material section.

$|dD^2/dt|$) with iso-butanol concentration. The initial burning period was not considered in the linearisation. Figure 6 shows the results.

Mean and standard deviations are shown. The horizontal lines represent the anticipated changes in droplet composition prior to ignition due to exposure of a droplet to air for 2 s, as measured by the method outlined in Appendix A. Preferential evaporation of n-heptane during this time enriches the droplet with iso-butanol. The effect is greatest at intermediate compositions but is generally small.

It is evident from Figure 6 that adding iso-butanol to n-heptane slows the burning process. A simple explanation draws on the classical theory of spherically symmetric droplet burning which shows that $K \propto 1/\rho_L$ [31]. Since the transfer number for iso-butanol is smaller than for n-heptane and the ratio of gas phase thermal conductivities to specific heats are about the same, the decrease in $K$ with increasing iso-butanol fraction could be caused by the increased mixture density from adding iso-butanol to the mixture. The iso-butanol density is considerably higher than n-heptane, Table 1. As a result, adding iso-butanol to heptane increases the mixture density relative to n-heptane and the burning rate should decrease which is consistent with Figure 6.

Shown in Figure 6 are selected colour images of the droplet at the indicated compositions to provide a qualitative measure of sooting propensity through flame brightness. N-heptane has a higher sooting propensity (and no oxygen) and burn rate compared to iso-butanol which produced less soot as a result of its oxygen content.

Some slight curvature is found in the $D^2$ histories which may be due to time-varying fuel compositions inside the droplet and/or droplet heating that persists throughout the burning history. Regarding the FSR, it shows non-quasi-steady behaviour. If burning were quasi-steady, the FSR would be independent of time [31]. The FSR generally decreases with increased iso-butanol addition as a result of iso-butanol's higher oxygen content. Radiative extinction may occur for alkane fuel droplets with initial diameters larger than 3 mm [13] as a result of substantial radiant heat loss the rate of which is proportional to $D_f^3$ [17]. However, the small droplet sizes in the present study can exhibit a diffusive extinction at very small diameters comparable to the fibre support diameters.

## 5. Comparison of simulations with experiments

Figures 5 and 6 show generally excellent agreement between experiment and computation concerning histories of droplet diameters. Some deviations are noted late in the burning process which are likely due to the increased difficulty of obtaining measurements for small droplets. The simulated evolutions of droplet diameter in Figure 5 generally predict quite well the experimentally measured values throughout the burning history over the whole composition range. Figure 6 further shows predicted burn rates in relation to the simulations and the agreement is very good.

In the development of the numerical model, soot formation was not included. It is interesting that the simulated droplet diameters are consistently lower than measured values in Figure 5. Soot formation is an endothermic process so a model which includes soot should slow the burning rate and, considering the relative placement of the data in Figure 5, reduce the difference between measured and predicted droplet diameters. However, there is no consistent trend of differences with composition shown in Figure 5. They are in any case small over the whole of the iso-butanol fractional loading in the mixture. The experiments showed only very faint soot shells that disappeared above about 20% iso-butanol loading for the atmospheric pressure conditions of the present experiment so the effect of sooting is not important. More likely is the effect of iso-butanol loading on the initial period of burning, or uncertainties in the database of thermal and transport properties used in the simulations. Again, though, differences are small in Figures 5 and 6.

Simulations of the flame diameter based on peak gas or OH concentrations bound the experimental measurement as shown in Figure 5. A flame diameter corresponding to the peak gas temperature is a good match of the flame diameter measurements early in the
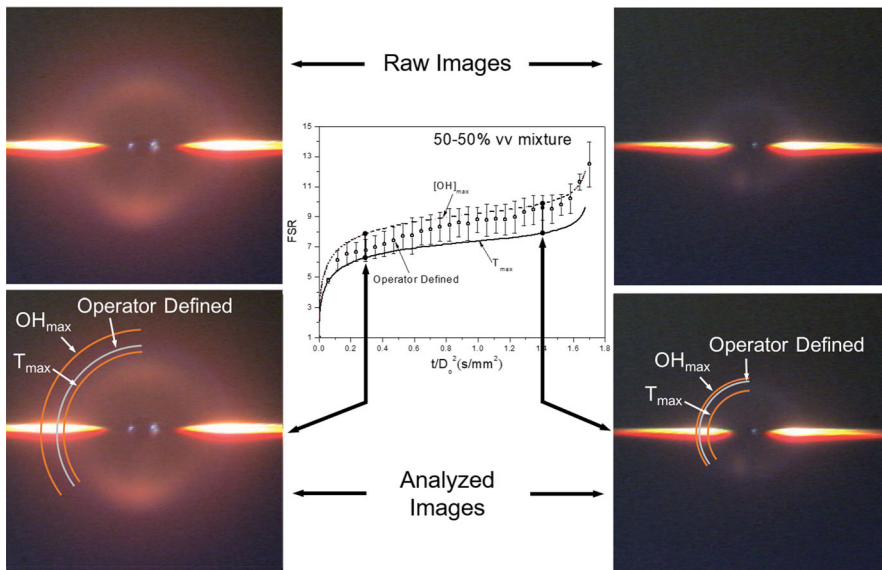


Figure 7. Comparisons of measured (operator-defined) flame diameters for a 50–50 mixture with predicted diameters defined by the locations of peak OH concentration ($OH_{max}$) and peak gas temperature ($T_{max}$). Arcs in the photos correspond to flame diameters, defined by peak OH or peak gas temperature values that would match predictions at the indicated scaled time. Also illustrated is a visual comparison of these definitions at $t/D_o^2 \sim 0.3$ s/mm$^2$ and $t/D_o^2 \sim 1.4$ s/mm$^2$.

burning history and a definition based on the peak OH concentration is better able to simulate flame diameter later in the burning history. As previously noted, the flame diameter is more difficult to measure than the droplet diameter. This contributes to the ambiguity of using the experimental measurements to determine the best definition of a flame diameter from the computational results.

To illustrate the challenge of determining the flame diameter from the video images, Figure 7 compares a particular 50/50 FSR profile measured from experiments to definitions of the flame diameter based on $T_{max}$ and $OH_{max}$.

Referencing the flame diameter with the blue zone surrounding a droplet (which is rather faintly visible in Figure 7), the results show that early in burning when the flame is close to the droplet, a $T_{max}$ flame definition does a reasonably good job of determining the flame location. The $T_{max}$ diameter appears to lie at approximately the midpoint of the outer blue zone while the $OH_{max}$ flame diameter is substantially outside it. Later in burning the $T_{max}$ definition is now well inside the blue zone while the $OH_{max}$ definition is nearer to the outer edge of the blue zone.

## 6. Implications concerning sooting

The potential for particulate emissions are concerns that factor into selecting an oxygenate as an alternative additive to fuel. While a soot model was not included in the simulations reported here, insights on soot formation can still be gained. A qualitative indication of sooting propensity is given by the concentration of acetylene ($C_2H_2$). This molecule is well-known for its importance in the creation of ring structures that lead to soot formation, and also soot growth. Figure 8 shows computed acetylene distributions for n-heptane (Figure 8(a)) and for an 80/20 mixture (Figure 8(b)). Measured flame and soot shell radii are also included in the figures along with the evolution of droplet diameters (data from Figures 5(a)).

From the computational results in Figure 8(a,b), the peak acetylene concentration is seen to lie just inside the 1350 K isotherm. This value is in the range found for laminar diffusion flames [32] and is referred to as the soot inception temperature (SIT). Specific values depend on fuel type and combustion configuration with the 1350 K value specific to the simulations and experiments reported here. Higher values considered in [32] would be closer to the flame and away from the measured soot shell radii or peak acetylene concentrations in Figure 8(a,b).

While the process of forming soot precursor particles (size of about 100 nm) could begin at the peak acetylene concentration, by the time the precursor particles are transformed into visible soot aggregates they are no longer at the location where they originated from because they will have moved inward by the thermophoretic forces acting on them. Concurrently, the evaporation-induced velocity exerts an outwardly directed drag force on aggregates. When these two forces are equal, the aggregate position (radius in Figure 8(a,b)) is stabilised and the aggregates collect to form the soot shell. This is a dynamic process due to the receding droplet surface. Figure 8(a,b) show that the shell radius is inside, and not at, the peak acetylene concentration.

Figure 8(c) shows that the acetylene concentration decreases by up to 40% with iso-butanol mixture fraction. This decrease forecasts a strong influence of iso-butanol mixture fraction on soot formation of the mixture. The decrease of flame brightness shown in Figure 4(b) does indicate less soot formed in the droplet burning process.
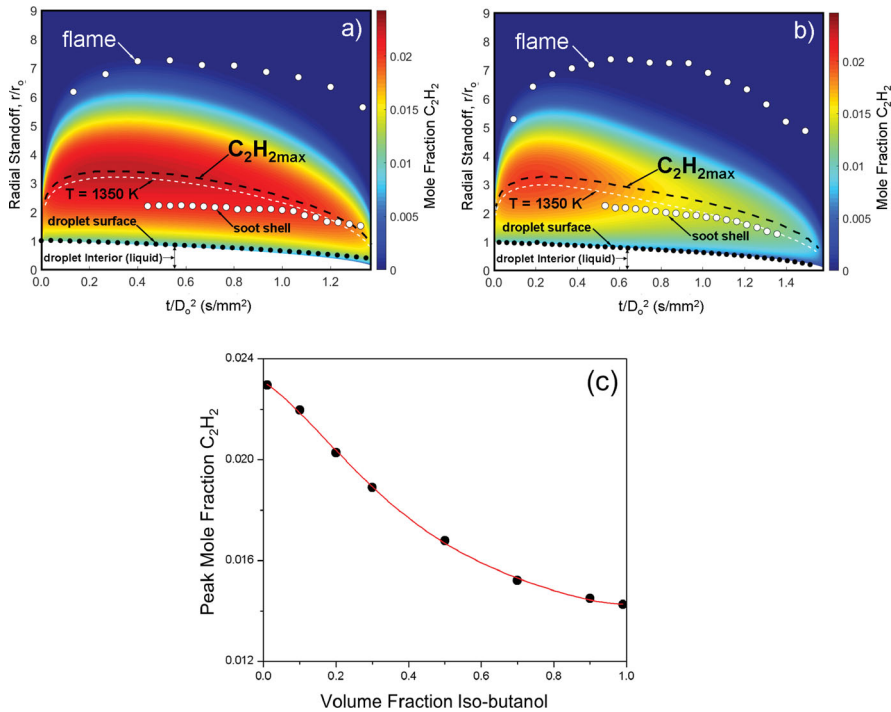
Figure 8. (a,b) Spatio-temporal evolution of mole fraction of acetylene ($C_2H_2$) for pure n-heptane (a) and an 80/20 n-heptane/iso-butanol mixture (b). The solid lines (a, b) correspond to the radii of peak carbon dioxide mole fractions. Filled circles are measured droplet, flame and soot-shell radii. The white dashed line corresponds to the 1350 K isotherm, suggested as a soot inception temperature [32]. Filled circles are measured droplet, flame and soot-shell radii. (c) Computed $C_2H_2$ peak concentration vs. composition.

## 7. Simulations of carbon dioxide concentration

The computed results also predict the concentrations of greenhouse gases (GHG) formed during the droplet burning process. Considering $CO_2$ as an example, Figure 9 shows simulated concentrations for both n-heptane (Figure 9(a)) and an 80/20 mixture (Figure 9(b)). This mixture concentration is sufficiently diluted of iso-butanol that soot still forms and the soot shell is visible in the experiments. At higher concentrations soot was not observed in the experiments (cf, Figure 4(a)) to the extent that a soot shell was not visible.

The peak $CO_2$ concentration is at the flame which is expected since it forms there, unlike for acetylene which forms well inside the flame. $CO_2$ diffuses from the flame both inwardly and outwardly.

Figure 9(c) shows the variation of peak $CO_2$ production with iso-butanol mixture fraction. The concentration increases, but tails off at about 0.4 mole fraction of iso-butanol and increases by only 3% as iso-butanol is added to n-heptane suggesting no strong deleterious effects from iso-butanol loading on GHG emissions. It is important to note, however, that such a conclusion is based on a burning process carried out at atmospheric pressure. High pressure burning will likely result in increased soot formation even for iso-butanol, and potentially higher concentrations of GHG emissions. The influence of pressure needs further analysis and experiments.
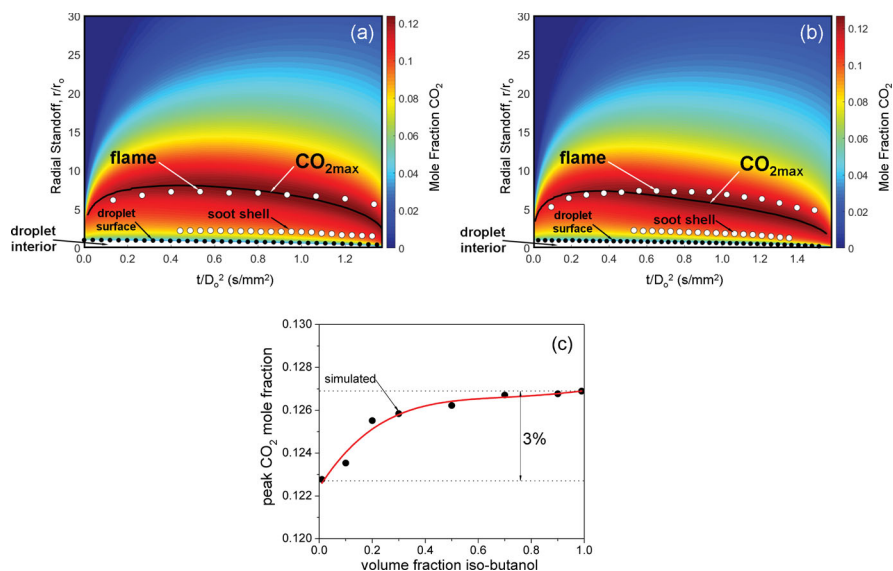
Figure 9. Spatio-temporal evolution of mole fraction of computed carbon dioxide ($CO_2$) for pure n-heptane droplet combustion (a) and an 80/20 n-heptane/iso-butanol mixture (b). The solid lines in (a, b) correspond to the radii of peak carbon dioxide mole fractions. Filled circles are measured droplet, flame and soot-shell radii. (c) $CO_2$ peak concentration vs. composition. The line is included to enhance the trends.

## 8. Conclusions

The atmospheric pressure results presented show that n-heptane and iso-butanol mixtures had droplet diameter squares that decreased nearly linearly with time during burning while the flame standoff ratio increased throughout burning. Increasing the iso-butanol fraction decreased the burning-rate because of the accompanying increase in the density of the iso-butanol compared to heptane. At the same time, increasing iso-butanol mixture fraction appreciably reduced the maximum acetylene mole fraction and the sooting tendency. The mechanism is consistent with carbon atoms in iso-butanol binding to oxygen atoms that cannot then be transformed into soot. Computational and experimental results exhibited generally very good agreement. The simulated flame diameters bounded the measurements using definitions of flame diameter based on the maximum temperature and maximum OH mole fraction.

With the simulations validated by the experiments, predictions of the peak acetylene concentrations as a soot precursor were made and found to occur very near the $1350\,K$ isotherm as a soot inception temperature. Moreover, simulated greenhouse gas concentrations ($CO_2$) were not appreciably changed with increasing iso-butanol concentration. As such, the results show a tradeoff with iso-butanol addition, namely that mixture droplets burn slower but produce less particulates and with little influence on formation of $CO_2$ as a representative greenhouse gas.

## 9. Nomenclature

*a*  major-axis
*b*  minor-axis

| | |
|---|---|
| $c_{p,g}$ | mean gas heat capacity |
| $c_{p,g,i}$ | heat capacity of gas species $i$ |
| $c_{p,L}$ | mean liquid heat capacity |
| $\mathfrak{D}_{L,g,i}$ | mass diffusivity of liquid ('L') or gas ('g') for species $i$ |
| $D$ | droplet diameter |
| $D_f$ | flame diameter |
| $D_o$ | initial droplet diameter |
| $E_{\min}$ | minimum energy |
| $f_{g,i}$ | fugacity of gas species $i$ |
| $f_{L,i}$ | fugacity of liquid species $i$ |
| $H_{g,i}$ | enthalpy of gas species $i$ |
| $h_{fg,i}$ | heat of vaporisation of species $i$ |
| $I$ | current |
| $K$ | burning rate |
| $k_g$ | mixture gas thermal conductivity |
| $k_L$ | mixture liquid thermal conductivity |
| $N_c$ | number of components (gas phase) |
| $n_{\text{samples}}$ | number of samples |
| $OH_{\max}$ | radial coordinate of max OH concentration |
| $q_R$ | radiative flux |
| $r$ | radial coordinate |
| $R_d$ | droplet radius |
| $R_\infty$ | reference volume radius |
| $T_L$ | liquid temperature |
| $T_g$ | gas temperature |
| $T_{\max}$ | radial coordinate of max gas temperature |
| $t$ | time |
| $\Delta t$ | time per sample |
| $V$ | voltage |
| $v_g$ | radial gas velocity |
| $v_L$ | radial liquid velocity |
| $V_{g,i}$ | gas diffusion velocity of species $i$ |
| $V_{L,i}$ | liquid diffusion velocity of species $i$ |
| $W_{\text{tot}}$ | mass flow rate |
| $Y_{g,i}$ | mass fraction of gas species $i$ |
| $Y_{L,i}$ | mass fraction of liquid species $i$ |
| $\rho_g$ | mean gas density |
| $\rho_{g,i}$ | partial density of gas species $i$ |
| $\rho_L$ | mean liquid density |
| $\tau$ | spark duration |
| $\omega_{g,i}$ | formation rate of gas species $i$ |

Subcripts

| | |
|---|---|
| $i$ | $i$th species $i = 1, 2, \ldots, N_c$ |
| $g$ | gas phase |
| $L$ | liquid phase |
| $n$ | $n$th sample $n = 1, 2, \ldots, n_{\text{samples}}$ |

## Acknowledgements

## Disclosure statement

No potential conflict of interest was reported by the author(s).

## Funding

## Supplemental data

Supplemental data for this article can be accessed http://10.1080/13647830.2020.1800823.

## References

[1] Office of Basic Energy Sciences, Office of Science and the Vehicle Technologies Program, Office of Energy Efficiency and Renewable Energy, U.S. Department of Energy. A Workshop To Identify Research Needs and Impacts in Predictive Simulation for Internal Combustion Engines (PreSICE); U.S. Department of Energy, Washington, DC, March 3, 2011. [https://www1.eere.energy.gov/vehiclesandfuels/pdfs/presice_rpt.pdf]

[2] National Research Council, *Transforming Combustion Research Through Cyberinfrastructure*, The National Academy Press, Washington, DC, 2011. [http://www.nap.edu/openbook.php?record_id = 13049]

[3] D. Pimentel and T.W. Patzek, *Ethanol production using corn, switchgrass, and wood; biodiesel production using soybean and sunflower*, Nat. Resour. Res 14(1) (2005), pp. 65–76.

[4] P. Miles, Efficiency Merit Function for Spark Ignition Engines: Revisions and Improvements Based on FY16–17 Research, Report No. DOE/GO-102018-5041, U.S. Department of Energy, 2018. [https://www.energy.gov/sites/prod/files/2018/02/f48/CoOptima%20Merit%20Function%20Report%20675842.pdf]

[5] J. Kolodzie and J. Scheib, *Bio-isobutanol: The next generation biofuel*. Hydrocarbon Process. Int Ed 91 (2012), pp. 79–85.

[6] S. Atusmi, T. Hanai and J.C. Liao, *Non-fermentative pathways for synthesis of branched-chain higher alcohols as biofuels*. Nature 451 (2008), pp. 86–89.

[7] Y. Ra and R.D. Reitz, *A reduced chemical kinetic model for IC engine combustion simulations with primary reference fuels*. Combust. Flame 155 (2008), pp. 713–738.

[8] K. Anand, Y. Ra, R.D. Reitz and B. Bunting, *Surrogate model development for fuels for advanced combustion engines*. Energy Fuels 25 (2011), pp. 1474–1484.

[9] H.J. Curran, P. Gaffuri, W.J. Pitz and C.K. Westbrook, *A comprehensive modeling study of n-heptane oxidation*. Combust. Flame 114 (1998), pp. 149–177.

[10] Y.C. Liu and C.T. Avedisian, *A comparison of the spherical flame characteristics of sub-millimeter droplets of binary mixtures of n-heptane/iso-octane and n-heptane/toluene with a commercial unleaded gasoline*. Combust Flame 159 (2012), pp. 770–783.

[11] C.K. Westbrook, W.J. Pitz and H.J. Curran, *Chemical kinetic modeling study of the effects of oxygenated hydrocarbons on soot emissions from diesel engines*. J. Phys. Chem. A 110 (2006), pp. 6912–6922.

[12] T.I. Farouk and F.L. Dryer, *Isolated n-heptane droplet combustion in microgravity: "cool flames" – two-stage combustion*. Combust. Flame 161 (2014), pp. 565–581.

[13] V. Nayagam, D.L. Dietrich, M.C. Hicks and F.A. Williams, *Cool-flame extinction during n-alkane droplet combustion in microgravity*. Combust. Flame 162 (2015), pp. 2140–2147.

[14] A. Stagni, A. Cuoci, A. Frassoldati, E. Ranzi and T. Faravelli, *Numerical investigation of soot formation from microgravity droplet combustion using heterogeneous chemistry*. Combust. Flame 189 (2018), pp. 393–406.

[15] A. Stagni, L. Esclapez, P. Govindaraju, A. Cuoci, T. Faravelli and M. Ihme, *The role of preferential evaporation on the ignition of multicomponent fuels in a homogeneous spray/air mixture*. Proc. Comb. Inst 36 (2017), pp. 2483–2491.

[16] T. Farouk, S.H. Won, and F. Dryer, *Investigating the role of preferential vaporization during submillimeter sized multicomponent jet fuel surrogate droplet combustion, paper no. G06, 11th U.S*. National Combustion Meeting, Western States Section, Combustion Institute, Pasadena, March 24–29, 2019.

[17] Y.C. Liu, Y. Xu, M.C. Hicks and C.T. Avedisian, *Comprehensive study of initial diameter effects and other observations on convection-free droplet combustion in the standard atmosphere for n-heptane, n-octane, and n-decane*. Combust. Flame 171 (2016), pp. 27–41.

[18] Y.C. Liu, Y. Xu, C.T. Avedisian and M.C. Hicks, *The effect of support fibers on microconvection in droplet combustion experiments*. Proc. Combust. Inst 35 (2015), pp. 1709–1716.

[19] C.L. Dembia, Y.C. Liu and C.T. Avedisian, *Automated data analysis of consecutive digital images from droplet combustion experiments by a MATLAB-based algorithm*. Image Anal. Stereol 31 (2012), pp. 137–148.

[20] T.I. Farouk, Y.C. Liu, A.J. Savas, C.T. Avedisian and F.L. Dryer, *Sub-millimeter sized methyl butanoate droplet combustion: Microgravity experiments and detailed numerical modeling*. Proc. Comb. Inst 34 (2013), pp. 1609–1616.

[21] A. Kazakov, J. Conley and F.L. Dryer, *Detailed modeling of an isolated, ethanol droplet combustion under microgravity conditions*. Combust. Flame 134 (2003), pp. 301–314.

[22] R.C. Reid, J.M. Prausnitz, and B.E. Poling, *The Properties of Gases and Liquids*. 4th ed. McGraw-Hill Book Company, New York, NY, 1987.

[23] A. Stagni, *Implementation of detailed chemistry in large-scale combustion computations*, Ph.D. thesis, Department of Chemistry, Materials, and Chemical Engineering, Politecnico di Milano, Piazza Leonardo da Vinci 32, 20133 Milano, 2016.

[24] A. Cuoci, A. Frassoldati, T. Faravelli and E. Ranzi, *OpenSMOKE + +: An object-oriented framework for the numerical modeling of reactive systems with detailed kinetic mechanisms*. Comput. Phys. Commun 192 (2015), pp. 237–264.

[25] OpenSMOKE + +, The CRECK Modeling Lab, Department of Chemistry, Materials, and Chemical Engineering, Politecnico di MilanoPiazza Leonardo da Vinci 32, 20133 Milano, ITALY; see also https://www.opensmokepp.polimi.it/

[26] E. Ranzi, A. Frassoldati, R. Grana, A. Cuoci, T. Faravelli, A.P. Kelley, and C.K. Law, *Hierarchical and comparative kinetic modeling of laminar flame speeds of hydrocarbon and oxygenated fuels*. Prog. Energy Combust. Sci 38 (2012), pp. 468–501.

[27] Y.C. Liu, F.E. Alam, Y. Xu, F.L. Dryer, C.T. Avedisian, and T.I. Farouk, *Combustion characteristics of butanol isomers in multiphase droplet configurations*. Combust. Flame 169 (2016), pp. 216–228.

[28] C.L. Yaws, *The Yaws Handbook of Physical Properties for Hydrocarbons and Chemicals*. 2nd ed.Gulf Professional Publishing, Waltham, MA., 2015.

[29] M.J. Assael, I. Bogdanou, S.K. Mylona, M.L. Huber, R.A. Perkins, and V. Vesovic, *Reference correlation of the thermal conductivity of n-heptane from the triple point to 600 K and up to 250 MPa*. J. Phys. Chem. Ref. Data 42 (2013), pp. 023101–0231-9.

[30] C.J. Mueller and G.C. Martin, Effects of Oxygenated Compounds on Combustion and Soot Evolution in a DI Diesel Engine: Broadband Natural Luminosity Imaging, SAE Technical Paper Series, paper no. 2002-01-1631.

[31] A. Crespo and A. Liñán, *Unsteady effects in droplet evaporation and combustion*. Combust. Sci. Tech. 11 (1975), pp. 9–18.

[32] R.A. Dobbins, *Soot inception temperature and the carbonization rate of precursor particles*. Combust. Flame 130 (2002), pp. 204–214.

## Appendix 1. Droplet vaporisation prior to an experiment

Exposure of a multicomponent fuel droplet to air during set-up of an experiment can produce a compositional change by preferential vaporisation. This effect can arise during the period between deploying a droplet onto the support fibres and the commencement of an experiment. The consequence would be a change in the fractional amount of components from the initially prepared mixture fractions.

A procedure outlined in was used to address this matter. It involves exposing droplets with arbitrary initial diameters to air and monitoring the time for the droplet to evaporate down to approximately 0.5 mm, which is the initial diameter of interest to this study. The droplet composition is then measured by GC/MS. Evaporation profiles for each fuel were developed this way and correlated with the exposure times. Figure A1 shows example evaporation profiles and associated GC/MS traces for the indicated initial mixture fractions.
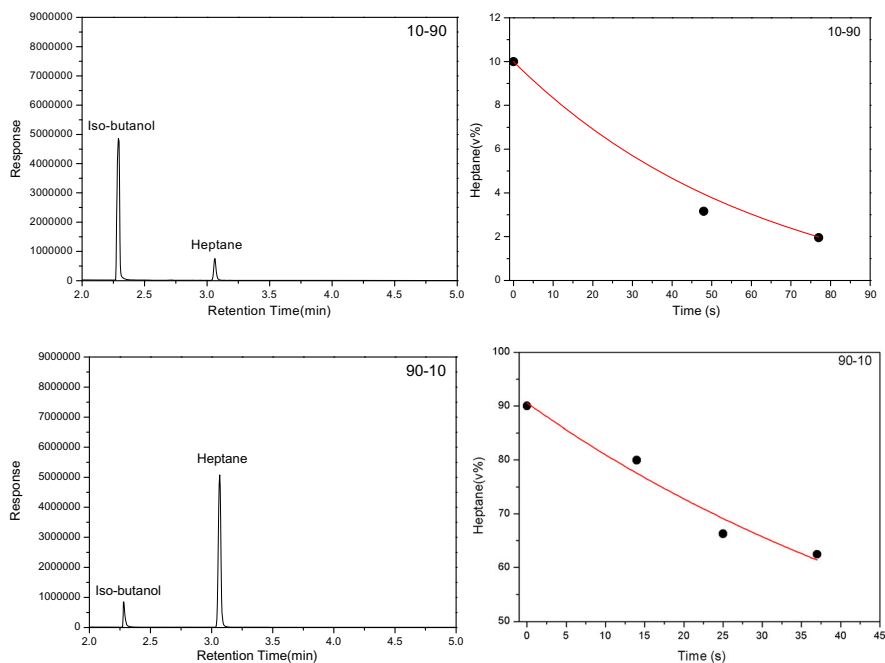


Figure A1.   (left-hand column) GC/MS traces of 10/90 and 90/10 heptane/iso-butanol mixtures showing the composition of droplets at the point of capture. (right-hand column) Evaporation profiles developed using GC/MS composition results and the exposure times before capture.

From figure A1, this pre-vaporisation effect can substantially change the droplet composition due to exposure to air prior to ignition. Exposure of a droplet to air for no more than 2 s or 3 s prior to ignition will alter the composition by only a few percent. The experimental procedure was developed with this consideration in mind. The initial conditions for the simulations were taken as the initially prepared mixture fractions.